Crystal-chemical investigation of the "cubic Al-Si spinel" issued from the thermal transformation of kaolinite and halloysite

Christelle Chauffeton, Gilles Wallez

Crystal-chemical investigation of the "cubic Al-Si spinel" issued from the thermal transformation of kaolinite and halloysite

Christelle Chauffeton [a, b, d], Gilles Wallez [a, c, d, *]

[a] Chimie ParisTech, PSL University, CNRS, Institut de Recherche de Chimie Paris, 75005 Paris, France

[b] Cité de la Céramique Sèvres-Limoges, 92310 Sèvres, France

[c] UFR 926, Sorbonne Université, 75005 Paris, France

[d] Centre de Recherche et Restauration des Musées de France, C2RMF, 75001 Paris, France

* corresponding author

gilles.wallez@sorbonne-universite.fr

Keywords

- kaolinite

- Al-Si spinel

- Rietveld analysis

- crystal structure

Highlights

- first determination of the crystal structure of the "Al-Si spinel"

- first quantitative assessment of the thermal transformation of kaolinite and halloysite

- evidence of the continuous nucleation of the "Al-Si spinel" beyond the collapse point of metakaolinite

Abstract

Since its discovery in 1959 as a transient nanocrystalline product of the thermal transformation of aluminum-rich clays, the so-called ”Al-Si spinel” has been the object of numerous studies aimed at determining its composition. In this work, samples obtained from fired kaolinite- and halloysite-containing clays were analyzed using X-ray diffraction, leading to conclude in a single cubic (space group *Fd*-3*m*) form, with an unvarying size of crystallites of 5 nm and a constant cell volume, typical of a transition alumina form. Trial-and-error Rietveld fitting procedure revealed a crystal structure consisting in an oxygen close packing and a disordered cation sublattice that differs from the known forms of spinel alumina. Rietveld quantitative phase analysis based on this model was successfully implemented on a series of fired halloysite clays, giving a first quantitative insight on the transformations in the 980-1260 °C range.

1. Introduction

Kaolin (a general term for kaolinite ($Al_2Si_2O_5(OH)_4$)-based clays) has been used worldwide for millennia in the manufacturing of ceramics, in particular porcelain. Naturally aluminum-rich and low in impurities, it is appreciated for its refractory properties and its whiteness. At high temperature, kaolinite undergoes a series of irreversible chemical and structural transformations known through an abundant literature [1-14]. At first, de-hydroxylation between 400 and 650 °C yields metastable metakaolinite $Al_2Si_2O_7$ that decomposes at 947 °C [15] into an amorphous silica-based phase and nanocrystalline needle-shaped aluminum-rich primary mullite, along with a nanocrystalline “Al-Si spinel” phase that will be the main topic of this work. A similar transformation is observed for related 1:1 phyllosilicate clays like halloysite, imogolite, dickite and allophane [5,10]. On further heating, secondary mullite grows by reaction between the spinel and the amorphous phase. This process goes together with a gradual substitution of silicon for aluminum in mullite and an increase of the crystals size. Although the growth of secondary mullite from pure kaolinite or a mixture with α-Al_2O_3 [7,14] starts around 1300 °C, this diffusion-based mechanism can be observed as low as 1000 °C in the presence of numerous metal oxides like Mg, Mn or Fe [4, 7, 12, 16-18]. These “mullitizers”, which are also of common occurrence in natural clays,

have long been used in industrial ceramics manufacturing to catalyze the conversion into mullite [19].

Conceivably, these irreversible thermal transformations which spread over hundreds of degrees could be monitored using X-ray diffraction (XRD) coupled to Rietveld analysis which offers an unparalleled potential in terms of crystal-chemical, microstructural and quantitative phases analysis (RQPA). However, though previous works endeavored exploring the thermal evolution of kaolinite through XRD, the phases quantification was relative [4] or based on calibration curves obtained by measuring the height or the surface of a single XRD peak on standards [3, 16, 20, 10]. It is noteworthy that the Rietveld method was never fully implemented in the study of these materials because of several difficulties: the presence of a glassy phase, the low crystallinity of primary mullite and, last but not least, the still unknown crystal structure and chemical composition of the Al-Si spinel, a point which remains subject to debate more than sixty years after its discovery.

Actually, the so-called phase was first reported in 1959 by Brindley and Nakahira [1] in the frame of the study of the kaolinite-mullite transformation. Diffuse XRD lines accounted for the presence of a nanocrystalline cubic phase, structurally related to spinel $MgAl_2O_4$. The irruption of this new phase in the intensively studied Al-Si-O system gave rise to divergent hypotheses concerning its formula - a point that still remains much debated. On the basis of the cubic symmetry and the cell parameter ($a \approx 7.90$ Å), Brindley and Nakahira pointed out the obvious kinship with γ-Al_2O_3, that occurs by heating boehmite and alumina gels, but structural relationships with metakaolinite led them to conjecture an Al_2O_3:SiO_2 = 2:3 mol ratio [1]. Using similar arguments, Low *et al.* [21] concluded in a 2:1 proportion, whereas Chakraborthy *et al.* measured a 2:3 ratio by elemental analyses [22].

Nevertheless, many early authors kept hanging on to a pure-alumina model, like Percival *et al.* who reached this conclusion from IR spectroscopy [23] and Léonard *et al.* from Radial Electron Density Distribution [24]. Brown *et al.* stated that "the spinel phase contains insufficient Si to be detected (…) and has a ^{27}Al NMR spectrum consistent with γ-Al_2O_3" [13]. This opinion would be tempered later on by some of these authors who detected a maximum of 3.9 w% SiO_2 (Al_2O_3:$SiO_2 \geq 14.5$:1) by ^{29}Si NMR [9], in contradiction with the maximum of 11.5 w% SiO_2 (4.5:1) found by Schneider *et al.* using the same method [25]. Analyzing an alkali-leached heated kaolinite [10] and a xerogel [26], Okada *et al.* found out the same 6:1 composition, in fair agreement with Sonuparlak *et al.*'s result (< 5.3:1) using EDS in an analytical TEM [11]. From TEM micrographs, Lee *et al.* observed a topotactic

relationship between metakaolinite and the spinel phase, and emitted the hypothesis that the Si content of the latter increased with temperature, as for mullite [8]. Conceivably, the nanometric size of the crystallites and their dispersion in the silica-rich glassy phase play a role in this discrepancy.

So, despite most studies - in particular, the most recent ones - agree with the fact that silicon, if any, only occurs in a faint amount in the Al-Si spinel, many questions still remain unaddressed: the precise chemical formula and its possible variability, the crystal structure and the amount in the products of decomposition of the clays. Whereas all these questions are usually addressed through XRD, no such study has ever been reported in the literature concerning the title compound. Indeed, several intrinsic impediments must be taken into account prior to an in-deep crystallographic investigation:

1- the nanometric size of the crystallites results in very diffuse diffraction peaks, amongst which only few are intense enough to be measured;

2- some of these peaks are blurred by the intense and irregular background due to the amorphous silica-rich phase;

3- the XRD pattern of the compound exhibits misleading similarities (apparent cubic symmetry, cell parameters and probably crystal structure) with those of η-Al_2O_3 (a = 7.906 Å [27,28]) and γ-Al_2O_3 (a = 7.938 Å [29], $(2V)^{1/3}$ = 7.898 Å [27] or 7.952 Å [30]);

4- silicon, if present in the compound, cannot be precisely distinguished from isoelectronic aluminum using X-ray;

5- probable cation/vacancy disorder - like in nanometric transition aluminas - may hamper the determination of the cation:anion ratio, hence of the composition.

2. Experimental

2.1. Starting materials and samples' preparation

The starting materials consisted in two minerals commonly used for the making of porcelain earthenware: a natural halloysite-rich clay originating from Les Eyzies, France (EZ in the following) and the kaolinite-rich ECC Standard Porcelain™, Imerys Minerals Ltd., UK (SP). The compositions in elemental oxides measured by X-ray fluorescence with a Bruker S1 Titan spectrometer are reported in Table 1. From preliminary XRD-Rietveld analysis, the EZ

clay contains 92 w% halloysite, *vs.* 84 w% kaolinite for the SP clay from the dealer's technical data chart.

Table 1. Elemental XRF assay of the Eyzies (EZ) and Standard Porcelain (SP) clays (oxygen not taken into account).

element	Si	Al	S	K	Rb	Mg	Ca
EZ	50.1(4)	45.7(5)	0.1	-	-	0.8(3)	0.1
SP	45.2(4)	38.9(4)	0.2(1)	4.1(2)	0.2	2.7(5)	1.8(2)
element	Sr	Ba	Ti	V	Cr	Mn	Fe
EZ	-	0.3	0.1	0.1	0.1	0.1	1.1(2)
SP	0.2	2.6(4)	0.1	-	-	0.1	3.9(2)

The clays were fired at various temperatures, with a particular attention paid to the domain of primary and secondary crystallization of mullite, between 950 and 1200 °C. The samples were put into an alumina crucible, introduced in the oven below 600 °C and heated at 300 °C.h^{-1} up to dwell temperature, then left during 1 h. The samples were ground into powders prior to XRD analysis.

2.2. X-ray powder diffraction and Rietveld analysis

The X-ray powder diffraction experiments were carried out in Bragg-Brentano configuration on a Panalytical Xpert Pro instrument with a Ge (111)-monochromated CuKα1 source and a PIXcel1D detector. The scans used for structure analyses were recorded over the 10-140 ° 2θ range, step 0.013 ° during 13 h. The Rietveld analyses were performed with the Fullprof suite [31]. Because of numerous faint and/or diffuse diffraction peaks, along with broad bumps due to the glassy phase, the background was fitted by interpolation between selected points without Bragg contribution of the spinel phase, at the same 2θ positions for all the samples. Various profile models were implemented depending on the nature of the crystalline phases.

The diffraction peaks of quartz, cristobalite and fluorite (used as an internal standard) were fitted with the pseudo-Voigt function and the Caglioti FWHM polynomial. Quartz's

structural data were refined to allow an optimal fit of this abundant phase, while those for cristobalite were taken from [32].

Concerning mullite, the Thompson-Cox-Hastings profile function [33] was implemented along with a uniaxial Lorentzian contribution to peak broadening to define a *hkl*-dependent FWHM model that took into account both the small size of the crystallites (particularly in the domain of primary crystallization) and their well-known elongation following the *c*-axis. Compared to the results obtained with the isotropic TCH function, this procedure allowed to reduce considerably the intensity residuals on the mullite peaks. Actually, the size effect can be considered to prevail according to previous Williamson-Hall [34] and Warren-Averbach [7] analyses which concluded in the limited contribution of the strains to the broadening. Mullite is a non-stoichiometric solid with general formula $Al_{4+2x}\ Si_{2-2x}\ O_{10-x}$, with x usually ranging from 0.2 to 0.9 (55 to 90 mol% Al_2O_3) [35, 36]. The site occupancy factors were refined in the secondary domain and kept fixed in the domain of primary crystallization where the diffracted intensities were not intense enough. In both cases, care was taken that the composition-sensitive *a*-cell edge and the Al:Si ratio remained in fair compliance with Fischer *et al.*'s relation [36].

As the Bragg peaks of the spinel phase appear symmetric and regular-shaped, a cubic symmetry was assumed, with the same *Fd*-3*m* space group as the $MgAl_2O_4$ archetype in compliance with the reflection conditions. However, due to the peaks' width, a slight lattice distortion like for γ-Al_2O_3 [27, 30] cannot be ruled out. The peaks were fitted with a pseudo-Voigt function. As will be shown in the following, the cations are scattered over four, partly-occupied sites. This disorder does not allow to refine the presence of silicon, if any. However, on the basis of the most recent research results and the analogy of the cell dimensions with those of transition aluminas, the present spinel phase can be thought of as pure alumina. The structure model was built from a fully occupied quasi close packing of oxygen atoms in 32*e* (*x*, *x*, *x*) position like in the spinel alumina models, then the cation array was determined by refining the occupancy of Al atoms in the five possible host sites (octahedral 16*c* (0, 0, 0) and 16*d* (1/2, 1/2, 1/2); tetrahedral 8*a* (3/8, 3/8, 3/8), 48*f* (*x*, 1/8, 1/8) and 8*b* (3/8, 3/8, 3/8)). After the 8*b* site was found to be empty, the total occupancy of the four other sites was constrained to comply with an Al:O = 2:3 atomic ratio.

An example of Rietveld plot can be seen on Fig. 1 (a comprehensive survey of the results is available in Table S1 (Supplementary Information)). As will be shown in the following, the growth of the secondary mullite coincides with the vanishing of the spinel phase. For this

reason, the most consistent - and arguably, reliable - results have been obtained from samples which only exhibit low amounts of mullite. Likewise, some samples still containing minor unidentified impurities in the low temperature domain yielded somewhat divergent structural parameters.

Furthermore, despite our efforts, the structural model may be impacted by the difficulties in measuring the areas of the spinel's diffuse Lorentzian peaks and cannot pretend to reach the usual standards in terms of precision.

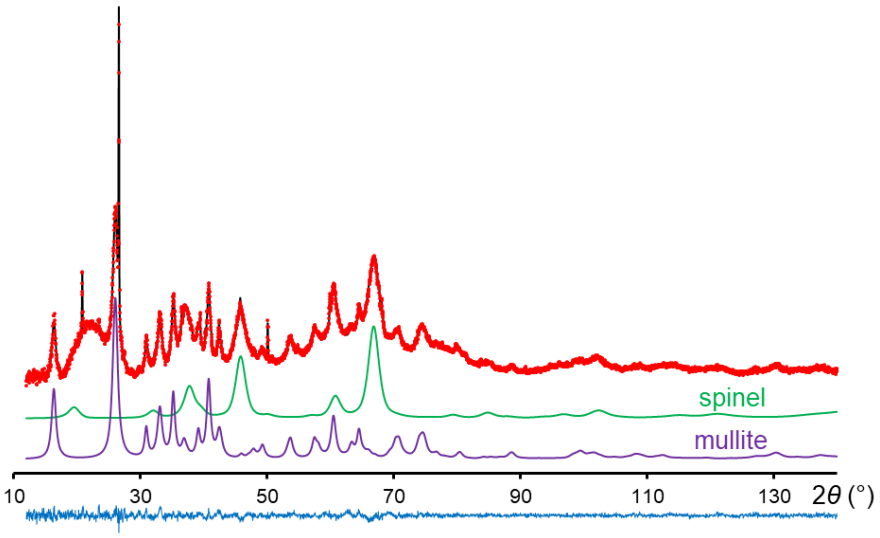

Fig. 1. Rietveld plot for sample SP_1080_1h: i_{obs} (red dots), i_{calc} (black), i_{obs} - i_{calc} (blue), and contributions of the spinel phase (green) and mullite (purple). Sharp peaks correspond to quartz. Sample holder baseline subtracted.

3. Results and Discussion

3.1. The crystal structure of the spinel phase

In the *Fd*-3*m* symmetry, the anion close packing provides two octahedral and three tetrahedral types of host sites for cations. The archetype spinel structure can be thought of as the interlocking of two similar sublattices, each made of [110] strips of equivalent octahedra bridged by two independent sets of tetrahedra. In an AB_2O_4 ordered model, octahedron-tetrahedron faces sharing only allows the occupation of one kind of octahedral (16*d*) and tetrahedral (8*a*) sites, but in transition aluminas, the cation deficiency ($Al_{2.667}O_4$ in a spinel-

type formulation) allows the simultaneous occupation of several octahedral and tetrahedral sites.

Concerning the present phase, the cation arrays refined for the diverse samples clearly exhibit strong similarities, in spite of discrepancies which often exceed the computed standard deviations (probably underestimated) but do not seem to be ascribable to the nature of the raw material, nor to the thermal treatment undergone (Fig. 2). Likewise, the Rietveld refinements did not reveal significant nor systematic variations of the cell parameter. Therefore, the following discussion will be based on a mean model derived from the data measured on samples containing high amounts of spinel, which consists in a cubic cell (a = 7.909(5) Å, similar to those of the pre-cited transition aluminas) with the atomic positions, site occupancy factors and Al-O bond lengths reported in Table 2.

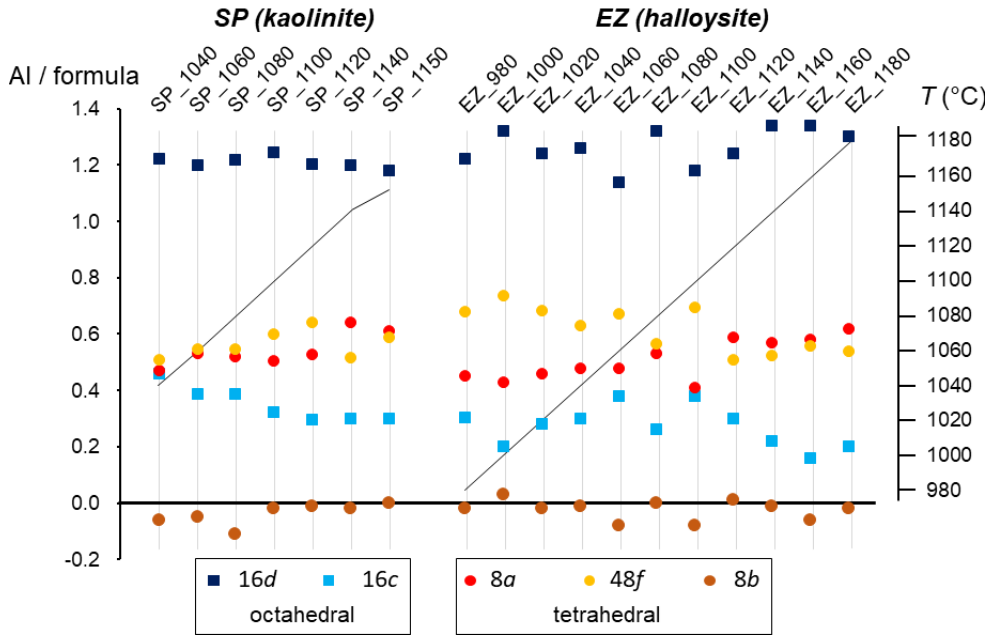

Fig. 2. Occupancy of the octahedral and tetrahedral sites of the spinel phase of selected samples, in number of Al atoms per $Al_{8/3}O_4$ formula.

Table 2. Averaged structural data for the spinel phase.

atom	site	coordinates	occupancy	atoms / $Al_{8/3}O_4$	B_{iso} (Å^2)	bond lengths (Å)
O	32*e*	(0.257(4), *x*, *x*)	1	4	0.8	

Al1	16*d*	(1/2, 1/2, 1/2)	0.62(3)	1.24(6)	0.6	1.92(3) x 6
Al2	16*c*	(0, 0, 0)	0.15(3)	0.30(6)	0.6	2.03(3) x 6
Al3	8*a*	(1/8, 1/8, 1/8)	0.52(7)	0.52(7)	0.6	1.81(3) x 4
Al4	48*f*	(0.368(8), 1/8, 1/8)	0.10(1)	0.60(6)	0.6	1.72(3) x 2 1.72(3) x 2
Al5	8*b*	(3/8, 3/8, 3/8)	0	0	-	1.62(3) x 4

The cation distribution amongst the octahedral and tetrahedral host sites is the main structural criterion that distinguishes the various forms of transition aluminas. In the present case, all the sites are partly occupied, except for tetrahedral 8*b*, which shares faces with both 16*d* and 16*c* and appears logically empty, like in all the known transition alumina structures. This four-site array accounts for a highly disordered structure in agreement with the nucleation-type formation mechanism. A comparison can be made with Smrčok *et al.*'s and Shirasuka *et al.*'s models for γ-Al_2O_3 [29] and η-Al_2O_3 [28] respectively: all these three forms feature the same occupied sites, but in γ-Al_2O_3, only 6 % of the cations (16*d*: 1.632, 16*c*: 0.056, 8*a*: 0.863, 48*f*: 0.114) are located off the 16*d*-8*a* regular positions *vs*. 39 % in η-Al_2O_3 (16*d*: 1.128, 16*c*: 0.540, 8*a*: 0.503, 48*f*: 0.498). As for the latter, the present compound (Table 2) exhibits a strongly (34 %) disordered cation array but any further comparison would be hazardous insofar as η-Al_2O_3 forms around 500 °C from bayerite or gelatineous pseudo-boehmite and decomposes as low as 900 °C [37].

3.2. Microstructure

The size of the crystallites can be assessed from the FWHM of the 400 and 440 reflections, the only intense ones. The Williamson-Hall analyses performed on 5 SP and 8 EZ samples with high spinel content (see Fig. S2 in Supplementary Information section) led to an average L = 5.0(5) nm value. Here also, no significant variations due to the starting clay or the thermal treatment were observed. This size is of the same order as Rozita *et al.*'s HRTEM and XRD measurements on commercial γ-Al_2O_3 powders (5-16 nm) [38].

3.3. Application to the Rietveld Quantitative Phase Analysis

The structural data set of the spinel phase was used to measure the thermal evolution of the phases issued from the transformation of halloysite. The EZ clay was preferred to the SP because of its lesser content in minor oxides, which delays the growth of secondary mullite and extends therefore the domain of existence of the spinel phase. The refinements were performed on the EZ_980 to _1260 samples admixed with 10 w% CaF_2 for the calibration of the diffracted intensities. The spinel pattern was modelled with the same profile function for all the samples. Fig. 3 features the weight ratios of the spinel phase, mullite, cristobalite and the amorphous phase calculated by residual, considering that these phases sum to 100 % (quartz (5.3(6) w%) is not taken into account).

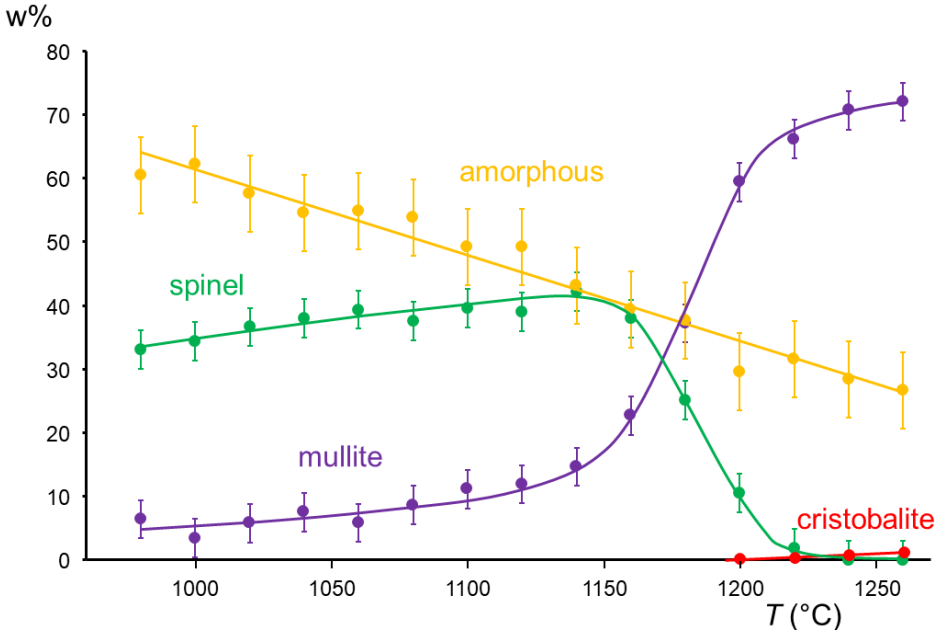

Fig. 3. Thermal evolution of the weight ratios of the spinel phase, mullite, cristobalite and amorphous phase issued from the EZ clay inferred from Rietveld quantitative phase analysis.

The domain of primary mullite crystallization (up to about 1140 °C) reveals a noteworthy phenomenon: the amount of spinel continues increasing all along, contrary to the common opinion that this phase directly stems from the collapse of metakaolinite. Indeed, it seems that a further nucleation occurs from the devitrification of the amorphous phase, but without growth according to the invariance of the crystallites' size, as expected from a mechanism occurring in an all-solid system. So, the spinel and the primary mullite develop independently until the secondary mullite begins growing, probably due to the increase of the

diffusion process which allows silica and alumina to react with each other. The onset and the end of this step match fairly with those of the spinel decrease. For comparison, the amount of the spinel phase issued from the SP clay starts decreasing as low as 1100 and vanishes around 1180 °C (Table S1), probably because of the presence of about 10 w% of secondary oxides *vs*. 3 w% in EZ. Beyond this temperature, mullite growth, which cannot be fed anymore by the spinel phase as a source of aluminum, may still occur from a direct reaction within the residual amorphous phase. Besides, faint amounts of cristobalite are observed starting from 1200 °C with both clays.

3.4. Stability of the spinel phase

The spinel phase issued from the transformation of kaolinite and halloysite is known to persist up to temperatures far beyond the domain of stability of pure "transition" aluminas generally obtained by dehydroxylation of alumina gels or hydrated minerals, as gibbsite-χ-κ, boehmite-γ-δ-θ and bayerite-η-θ transformation routes all end with the collapse of the low-density spinels into the massive and stable α-form (corundum) between 1050 and 1100 °C [37]. The existence of these transition aluminas up to these high temperatures – an asset for their use as catalysts – is generally ascribed to the high specific surface that results from their synthesis route.

However, studies carried out during the past decades on the substitution of various oxides in transition aluminas highlighted a stabilizing effect that can be ascribed to their higher solubility in a spinel-type structure than in α-Al_2O_3 [39, 40]. Both iso- and aliovalent substitutions are favored by the lacunary cation sublattice and the presence of tetrahedral host sites, whereas in α-Al_2O_3, only octahedral sites can be occupied. The case of silicon oxide is of particular interest for the present study because its presence in faint amounts in the "Al-Si spinel" cannot be excluded. Computational studies [41-43] all concluded that Si in low concentrations (0-5 at%) should take place into tetrahedral sites and build stronger bonds than Al, thus increasing the stiffness and the stability of the spinel framework. It is noteworthy however that the real solubility of Si in these phases remains unknown. Firing an Al_2O_3:SiO_2 = 95:5 w% gel in the frame of the earliest experiment-based study, Chakravorty & Ghos reported γ-Al_2O_3 and nanometric "Al-Si spinel" at 1000 °C, which entirely transformed into α-Al_2O_3 and mullite after 1 h at 1200 °C [44]. Mekasuwandumrong *et al.* investigated the

effect of SiO_2 on solvothermal χ-Al_2O_3, but they only observed a retardation of 100 °C for the formation of α-Al_2O_3 [45].

4. Conclusion

Although the composition of the so-called "Al-Si spinel" remains a pending issue, its crystal structure solved by the Rietveld method can be described as a new type of cubic transition alumina with a high cation/vacancy disorder. Despite approximate, the structural model – the first one proposed more than sixty years after the discovery of the phase - allowed to measure the ratios of the phases issued from the transformation of an halloysite-rich clay, but the same process can be implemented for other minerals containing 1:1 phyllosilicates, in particular to assess the effect of minor oxides, known to act as mullitizers, or in experimental archaeology for the determination of the thermal treatment undergone by an earthenware artifact.

From a more fundamental point of view, it is worth noting that the spinel observed in the present work does not seem to "collapse" by itself, but rather reacts with the silica-rich glassy phase according to the simultaneous growth of secondary mullite. Arguably, this spinel form exhibits a higher thermal stability compared to all the transition aluminas, whether pure or doped with silicon. Although this study does not pretend to address this issue, further works could be intended in order to investigate the role played by some of the physico-chemical peculiarities in its stability, that is, the crystal structure based on an original cation array, the very small size of the crystallites and their dispersion in the glassy matrix.

Acknowledgements

The authors wish to thank Dr Atika Chemmi, Head of the Applied Research Department of the *Manufacture Nationale de Sèvres*, France, for selecting and providing the clay samples and Dr Thibault Charpentier, Research Director at the CEA, France for his kind help in trying to solve the issue of the "Al-Si spinel" composition. *CC* is grateful to the *Fondation Bettencourt-Schueller* and the *Cité de la Céramique Sèvres-Limoges*, France for founding her work in the frame of her PhD thesis.

Supplementary information

The CIF file of the averaged crystal structure, details concerning the structure and lattice parameters of the spinel phase in the studied samples, a comparison with the known structural forms of transition aluminas, the Williamson-Hall plot and the calculated XRD pattern of the averaged crystal structure are provided as Supplementary Information.

References

[1] G.W. Brindley, M. Nakahira, Kaolinite–Mullite Reaction Series III, The High-Temperature Phases, J. Am. Ceram. Soc. 42 (1959) 319-24. https://doi.org/10.1111/j.1151-2916.1959.tb14316.x

[2] A. Ortega, M. Macias, F.J. Gotor, The Multistep Nature of the Kaolinite Dehydroxylation: Kinetics and Mechanism, J. Am. Ceram. Soc. 93 (2010) 197-203. https://doi.org/10.1111/j.1551-2916.2009.03328.x

[3] A.K. Chakravorty, D.K. Ghosh, Kaolinite-Mullite Reaction Series: The Development and Significance of a Binary Aluminosilicate, J. Am. Ceram. Soc. 74 (1991) 1401-06. https://doi.org/10.1111/j.1151-2916.1991.tb04119.x

[4] A.H. De Aza, X. Turrillas, M.A. Rodriguez, T. Duran, P. Pena, Time-resolved powder neutron diffraction study of the phase transformation sequence of kaolinite to mullite, J. Eur. Ceram. Soc. 34 (2014) 1409-1421. https://doi.org/10.1016/j.jeurceramsoc.2013.10.034.

[5] J.F. Duncan, K.J.D. MacKenzie, P. K. Foster, Kinetics and Mechanism of High-Temperature Reactions of Kaolinite Minerals, J. Am. Ceram. Soc. **52** (1969) 74-77. https://doi.org/10.1111/j.1151-2916.1969.tb13343.x

[6] A. Gualtieri , M. Bellotto, G. Artioli, S.M. Clark, Kinetic Study of the Kaolinite-Mullite Reaction Sequence. Part II: Mullite Formation, Phys. Chem. Minerals 22 (1995) 215-222. https://doi.org/10.1007/BF00202254

[7] M.A. Sainz, F.J. Serrano, J. M. Amigo, J. Bastida, A. Caballero, XRD Microstructural Analysis of Mullites Obtained from Kaolinite-Alumina Mixtures, J. Eur. Ceram. Soc. 20 (2000) 403-12. https://doi.org/10.1016/S0955-2219(99)00183-1

[8] S. Lee, Y.J. Kim, H.S. Moon, Phase Transformation Sequence from Kaolinite to Mullite Investigated by an Energy-Filtering Transmission Electron Microscope, J. Am. Ceram. Soc. 82 (1999) 2841-48. https://doi.org/10.1111/j.1151-2916.1999.tb02165.x

[9] K.J.D. MacKenzie, J.S. Hartman, K. Okada, MAS NMR Evidence for the Presence of Silicon in the Alumina Spinel from Thermally Transformed Kaolinite, J. Am. Ceram. Soc., 79 (1996) 2980-82. https://doi.org/10.1111/j.1151-2916.1996.tb08738.x

[10] K. Okada, N. Ōtsuka, J. Ossaka, Characterization of Spinel Phase Formed in the Kaolin-Mullite Thermal Sequence, J. Am. Ceram. Soc. 69 (1986) C-251–C-253. https://doi.org/10.1111/j.1151-2916.1986.tb07353.x

[11] B. Sonuparlak, M. Sarikaya, I.A. Aksay, Spinel Phase Formation During the 980 °C Exothermic Reaction in the Kaolinite-to-Mullite Reaction Series, J. Am. Ceram. Soc. 70 (1987) 837-42. https://doi.org/10.1111/j.1151-2916.1987.tb05637.x

[12] S.M. Johnson, J.A. Pask, J.M. Moya, Influence of impurities on high-temperature reactions of kaolinite, J. Am. Ceram. Soc. 65 (1980) 31-35. https://doi.org/10.1111/j.1151-2916.1982.tb09918.x

[13] I.W.M. Brown, K.J.D. MacKenzie, M.E. Bowden, R.H. Meinhold, Outstanding Problems in the Kaolinite-Mullite Reaction Sequence Investigated by ^{29}Si and ^{27}Al Solid-State Nuclear Magnetic Resonance: High-Temperature Transformations of Metakaolinite, J. Am. Ceram. Soc., 68 (1985) 298-301. https://doi.org/10.1111/j.1151-2916.1985.tb15228.x

[14] K.C. Liu, G. Thomas, A. Caballero, J.S. Moya, S. De Aza, Mullite formation in kaolinite-α-alumina, Acta Metall. Mater. 42 (1994) 489-495. https://doi.org/10.1016/0956-7151(94)90503-7

[15] P. Ptaček, F. Šoukal, T. Opravil, M. Novasková, J. Havlica, J. Brandštetr, The kinetics of Al-Si spinel phase crystallization from calcined kaolin, J. Solid State Chem. 183 (2010) 2565-2569. https://doi.org/10.1016/j.jssc.2010.08.030

[16] H. Shin, C.S. Kim, S.N. Chang, Mullitization from a Multicomponent Oxide System in the Temperature Range 1200°–1500°C, J. Am. Ceram. Soc. 83 (2000) 1237-40. https://doi.org/10.1111/j.1151-2916.2000.tb01360.x

[17] A. Yamuna, S. Devanarayanan, M. Lalithambika, Phase-Pure Mullite from Kaolinite, J. Am. Ceram. Soc. 85 (2002) 1409-13. https://doi.org/10.1111/j.1151-2916.2002.tb00289.x

[18] A. Odaka, T. Yamaguchi, T. Fujita, S. Taruta, K. Kitajima, Cation dopant effect on phase transformation and microstructural evolution in M^{2+}-substituted gamma-alumina powders, J. Mater. Sci. 43 (2008) 2713–2720. https://doi.org/10.1007/s10853-008-2485-5

[19] C.W. Parmelee, A.R. Rodriguez, Catalytic Mullitization of Kaolinite by Metallic Oxides, J. Am. Ceram. Soc. 25 (1942) 1-10. https://doi.org/10.1111/j.1151-2916.1942.tb14286.x

[20] Y.F. Chen, M.C. Wang, M.H. Hon, Kinetics of secondary mullite formation in kaolin-Al_2O_3 ceramics, Scripta Mater. 51 (2004) 231-235. https://doi.org/10.1016/j.scriptamat.2004.04.013

[21] I.M. Low, R.R. McPherson, The structure and composition of Al-Si spinel, J. Mater. Sci. Lett. 7 (1988) 1196-1198.

[22] A.K. Chakraborthy, D.N. Ghosh, Reexamination of Kaolinite–Mullite Reaction Series, J. Am. Ceram. Soc. 61 (1978) 170-73. https://doi.org/10.1111/j.1151-2916.1978.tb09264.x

[23] H.J. Percival, J.F. Duncan, P.K. Foster, Interpretation of the kaolinite-mullite reaction sequence from infrared absorption spectra, J. Am. Ceram. Soc. 57 (1974) 57-61. https://doi.org/10.1111/j.1151-2916.1974.tb10813.x

[24] A.J. Léonard, Structural Analysis of the Transition Phase in the Kaolinite-Mullite Thermal Sequence, J. Am. Ceram. Soc. 60 (1977) 37-43. https://doi.org/10.1111/j.1151-2916.1977.tb16089.x

[25] H. Schneider, D. Voll, B. Saruhan, M. Schmücker, T. Schaller, A. Sebald, Constitution of the γ-Alumina Phase in Chemically-Produced Mullite Precursors, J. Eur. Ceram. Soc. 13 (1994) 441-48. https://doi.org/10.1016/0955-2219(94)90022-1

[26] K. Okada, N. Ōtsuka, Characterization of the spinel phase from SiO_2-Al_2O_3 xerogels and the formation process of mullite, J. Am. Ceram. Soc. 69 (1986) 652-56. https://doi.org/10.1111/j.1151-2916.1986.tb07466.x

[27] D. Li, B.H. O`Connor, G.I.D. Roach, J.B. Cornell, Structural models of eta- and gamma-aluminas by X-ray Rietveld refinement, Acta Crystallogr. A 46 (1990) C61a.

[28] K. Shirasuka, H. Yanagida, G. Yamaguchi, The preparation of eta alumina and its structure, Yogyo Kyokaishi Shi (J. Ceram. Assoc. Jpn.) 84 (1976) 610-613. https://doi.org/10.2109/jcersj1950.84.976_610

[29] Ľ. Smrčok, V. Langer, J. Křesťan, Gamma-alumina: a single-crystal X-ray diffraction study, Acta Crystallogr. C 62 (2006) i83-i84. https://doi.org/10.1107/S0108270106026850

[30] G. Paglia, C.E. Buckley, A.L. Rohl, B.A. Hunter, R.D. Hart, J.V. Hanna, L.T. Byrne, Tetragonal structure model for boehmite-derived gamma-alumina, Phys. Rev. B: Condens. Matter. Mater. Phys. 68 (2003) 1-11. https://doi.org/10.1103/PhysRevB.68.144110

[31] J. Rodriguez-Carvajal, FULLPROF: A Program for Rietveld Refinement and Pattern Matching Analysis, Abstracts of the Satellite Meeting on Powder Diffraction of the XV Congress of the IUCr, Toulouse, France (1990), p. 127.

[32] W.A. Dollase, Reinvestigation of the structure of low cristobalite, Z. Kristallogr. 121 (1965) 369-377. https://doi.org/10.1524/zkri.1965.121.5.369

[33] P. Thompson, D.E. Cox, J.B. Hastings, Rietveld refinement of Debye-Scherrer synchrotron X-ray data from Al_2O_3, J. Appl. Cryst. 20 (1987) 79-83.

https://doi.org/10.1107/S0021889887087090

[34] O. Castelein, R. Guinebretière, J.P. Bonnet, P. Blanchart, Shape, size and composition of mullite nanocrystals from a rapidly sintered kaolin, J. Eur. Ceram. Soc. 21 (2001) 2369–2376. https://doi.org/10.1016/S0955-2219(01)00211-4

[35] H. Schneider, J. Schreuer, B. Hildmann, Structure and properties of mullite – A review, J. Eur. Ceram. Soc. 28 (2008) 329-344. https://doi.org/10.1016/j.jeurceramsoc.2007.03.017

[36] R. X. Fischer, H. Schneider, D. Voll, Formation of aluminum rich 9:1 mullite and its transformation to low alumina mullite upon heating, J. Eur. Ceram. Soc. 16 (1996) 109-113. https://doi.org/10.1016/0955-2219(95)00139-5

[37] K. Wefers, C. Misra, Alcoa Technical Paper No. 19, revised (1987). Alcoa Laboratories, Pittsburg, PA, USA.

[38] Y. Rozita, R. Brydson, A. J. Scott, An investigation of commercial gamma-Al_2O_3 nanoparticles, J. Phys. 241 (2010) 012096. doi:10.1088/1742-6596/241/1/012096

[39] K. Okada, A. Hattori, T. Taniguchi, A. Nukui, R.N. Das, Effect of divalent cation additives on the gamma-Al_2O_3-to-alpha-Al_2O_3 phase transition, J. Am. Ceram. Soc. 83 (2000) 928-932. https://doi.org/10.1111/j.1151-2916.2000.tb01296.x

[40] F. Maglia, S. Gennari, Energetics of aluminum vacancies and incorporation of foreign trivalent ions in γ-Al_2O_3: an atomistic simulation study, J. Am. Ceram. Soc. 91 (2008) 283-290. https://doi.org/10.1111/j.1551-2916.2007.02149.x

[41] F. Nahif, D. Music, S. Mraz, M. to Baben, J.M. Schneider, *Ab initio* study of the effect of Si on the phase stability and electronic structure of γ- and α-Al_2O_3, J. Phys.: Condens. Matter 25 (2013) 125502. doi:10.1088/0953-8984/25/12/125502

[42] K. Jiang, D. Music, K. Sarakinos, J. M. Schneider, Ab initio study of effects of substitutional additives on the phase stability of γ-alumina, J. Phys.: Condens. Matter 22 (2010) 505502. doi:10.1088/0953-8984/22/50/505502

[43] J.M. Andersson, E. Wallin, V. Chirita, E.P. Münger, U. Helmersson, *Ab initio* calculations on the effects of additives on alumina phase stability, Phys. Rev. B 71 (2005) 014101. https://doi.org/10.1103/PhysRevB.71.014101

[44] A.K. Chakravorty, D.K. Ghosh, Crystallization behavior of Al_2O_3 in the presence of SiO_2, J. Am. Ceram. Soc. 70 (1987) C-46-C-48. https://doi.org/10.1111/j.1151-2916.1987.tb04962.x

[45] O. Mekasuwandumrong, P. Tantichuwet, C. Chaisuk, P. Praserthdam, Impact of concentration and Si doping on the properties and phase transformation behavior of nanocrystalline alumina prepared via solvothermal synthesis, Mater. Chem. Phys. 107 (2008) 208-214. https://doi.org/10.1016/j.matchemphys.2007.06.060

Supplementary information section

Table S1. Main parameters concerning the spinel phase issued from the Rietveld analyses: spinel/mullite w/w ratio, oxygen atom coordinate *x*, site occupancy factors of aluminum in octahedral (16*d* and 16c) and tetrahedral (8*a*, 48*f* and 8*b*) sites, cell parameter *a* (Å), full width at half maximum of main 400 and 440 peaks (W_{400} and W_{440}, °) and R_{Bragg} reliability factor (%). Shaded samples were not taken into account in the determination of the average spinel model due to too faint intensities or to the presence of impurity peaks.

sample	*spin / mull*	x_O	x_{48f}	occ. 16*d*	occ. 16*c*	occ. 8*a*	occ. 48*f*	occ. 8*b**	*a*	W_{400}	W_{440}	R_{Bragg}
SP 1000_1h	5.50	0.2628(6)	0.364(3)	0.61(1)	0.23(1)	0.47(3)	0.085(5)	-0.09(3)	7.911(1)	1.97	2.40	0.70

SP 1040_1h	1.84	0.2628(6)	0.364(3)	0.61(1)	0.23(1)	0.47(3)	0.085(5)	-0.09(3)	7.911(1)	2.21	2.11	2.20
SP 1060_1h	1.26	0.2603(5)	0.365(2)	0.599(8)	0.194(8)	0.53(2)	0.091(3)	-0.09(3)	7.910(1)	2.02	1.99	0.37
SP 1080_1h	1.25	0.2599(5)	0.364(3)	0.607(8)	0.194(4)	0.519(9)	0.091(3)	-0.07(2)	7.909(1)	1.99	2.02	0.72
SP 1100_1h	1.14	0.2596(6)	0.364(3)	0.622(7)	0.161(4)	0.503(9)	0.100(2)	-0.02(2)	7.910(1)	1.95	1.97	0.38
SP 1120_1h	0.95	0.2598(6)	0.362(3)	0.602(7)	0.148(4)	0.526(9)	0.107(2)	-0.02(1)	7.913(1)	1.85	2.00	0.32
SP 1140_1h	0.58	0.2618(7)	0.359(3)	0.60(1)	0.15(1)	0.64(2)	0.086(4)	-0.02(2)	7.916(1)	1.88	1.99	0.55
SP 1150_1h	0.26	0.266(1)	0.350(4)	0.59(2)	0.15(1)	0.61(2)	0.098(6)	0.00(3)	7.922(1)	*f*	*f*	1.05
SP 1160_1h	0.27	*f*	*f*	*f*	*f*	*f*	*f*	*f*	-	*f*	*f*	1.05
SP 1180_1h	0.03	*f*	*f*	*f*	*f*	*f*	*f*	*f*	-	*f*	*f*	5.7
sample	*spin / mull*	x_O	x_{48f}	occ. 16*d*	occ. 16*c*	occ. 8*a*	occ. 48*f*	occ. 8*b**	*a*	W_{400}	W_{440}	R_{Bragg}
EZ 960_1h	4.40	*f*	*f*	*f*	*f*	*f*	*f*	*f*	7.917(7)	*f*	*f*	7.66
EZ 980_1h	5.15	0.2539(9)	0.375(2)	0.61(1)	0.152(7)	0.45(1)	0.113(4)	-0.02(2)	7.906(1)	1.93	2.15	0.76
EZ 1000_1h	10.00	0.2526(8)	0.375(2)	0.66(1)	0.10(1)	0.39(3)	0.125(5)	0.03(3)	7.909(1)	1.90	2.05	0.90
EZ 1020_1h	6.30	0.2534(8)	0.377(2)	0.62(1)	0.14(1)	0.46(2)	0.114(4)	-0.02(2)	7.905(1)	1.89	2.13	0.72
EZ 1040_1h	5.05	0.2536(8)	0.376(2)	0.63(1)	0.15(1)	0.48(2)	0.104(4)	-0.01(2)	7.904(1)	1.91	2.09	0.58
EZ 1060_1h	6.70	0.2576(7)	0.372(2)	0.56(1)	0.19(1)	0.48(2)	0.112(4)	-0.02(3)	7.907(1)			0.95
EZ 1080_1h	4.32	0.2531(8)	0.378(2)	0.669(9)	0.114(6)	0.49(1)	0.101(3)	0.00(2)	7.902(1)	1.90	2.07	0.91
EZ 1100_1h	3.54	0.2574(5)	0.363(2)	0.587(6)	0.193(4)	0.407(8)	0.117(2)	-0.08(5)	7.906(1)			0.67
EZ 1120_1h	3.27	0.254(1)	0.377(2)	0.62(1)	0.15(1)	0.59(2)	0.085(4)	0.01(2)	7.908(1)	1.79	1.87	0.86
EZ 1140_1h	2.87	0.2524(9)	0.378(2)	0.67(1)	0.10(1)	0.57(2)	0.087(3)	-0.01(2)	7.902(1)	1.83	1.96	0.73
EZ 1160_1h	1.67	0.2535(9)	0.376(2)	0.67(1)	0.08(1)	0.58(2)	0.093(4)	-0.06(3)	7.902(1)	1.83	2.02	0.71
EZ	0.68	0.258(1)	0.369(3)	0.65(2)	0.09(1)	0.62(2)	0.089(6)	-0.02(2)	7.902(1)	1.92	2.09	1.24

1180_1h												
EZ 1200_1h	0.18	*f*	*f*	*f*	*f*	*f*	*f*	*f*	-	*f*	*f*	3.24
EZ 1220_1h	0.03	*f*	*f*	*f*	*f*	*f*	*f*	*f*	-	*f*	*f*	7.37

* the occupancy of the "empty" 8*b* site was refined freely, whereas those of the other sites were constrained to comply with a global Al_2O_3 formula.

"*f*" means fixed for insufficient intensity.

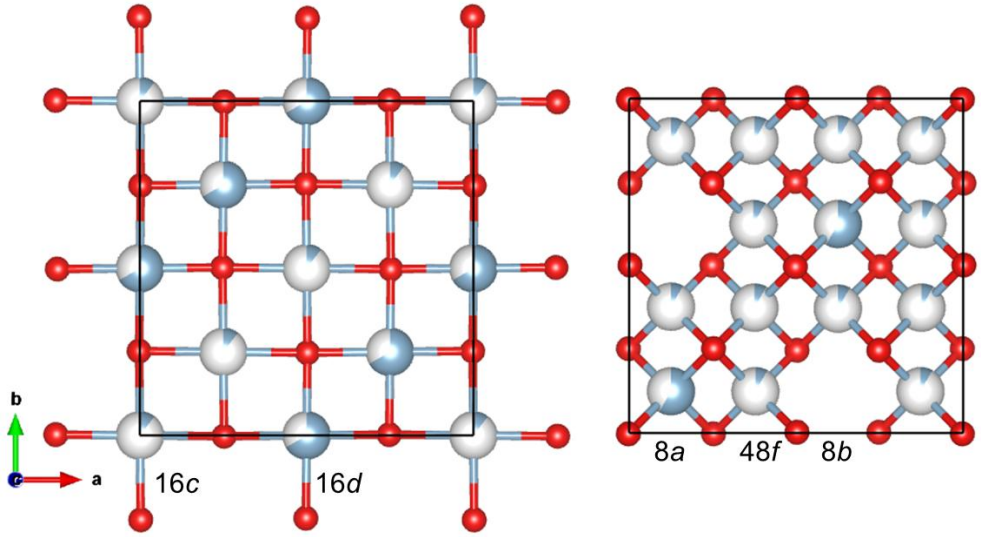

Fig. S1. Occupancy scheme of the cation sites: octahedral (left) and tetrahedral (right).

Table S2. Comparison between the cations arrays in the averaged "Al-Si spinel" model and in some transition aluminas ((T) refers to a tetragonal cell distortion).

	16*c* 0, 0, 0	16*d* ½, ½, ½	48*f* *x*, 1/8, 1/8	8*a* 1/8, 1/8, 1/8	8*b* 3/8, 3/8, 3/8
γ-Al_2O_3 (T) [Li]	0	2.000	0	0.667	0
γ-Al_2O_3 [29]	0.056	1.632	0.114	0.863	0
γ-Al_2O_3 [Saraswati]	0	2.000	0	0.667	0

η-Al_2O_3 [27]	0	0.667	0	2.000	0
η-Al_2O_3 [28]	0.540	1.128	0.498	0.503	0
Al-Si spinel (this work)	0.30(6)	1.24(6)	0.60(6)	0.52(7)	0

[Saraswati] V. Saraswati, G.V.N. Rao, X-ray diffraction in gamma-alumina whiskers, J. Cryst. Growth 83 (1987) 606.

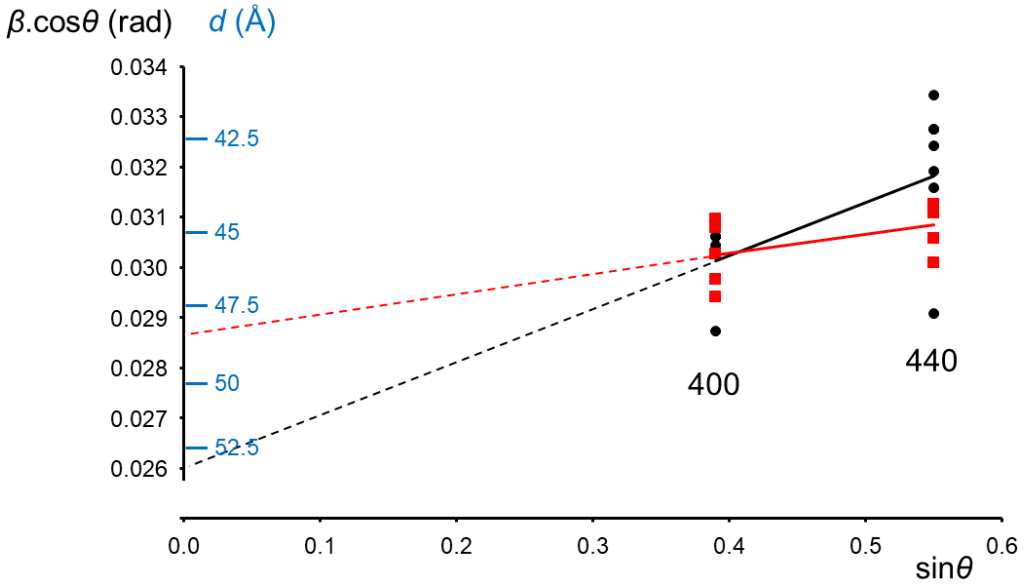

Fig. S2. Williamson-Hall plot based on the 400 and 440 reflections of the SP (red) and EZ (black). The lines are plotted from the mean values for each group of points.

Table S3. Calculated XRD diagram of the averaged spinel phase at $\lambda_{CuK\alpha1}$ = 1.5405 Å.

h	*k*	*l*	*d* (Å)	2θ (°)	*I* (‰)
1	1	1	4.566	19.42	67
2	2	0	2.796	31.98	58
3	1	1	2.385	37.69	357
2	2	2	2.283	39.44	101
4	0	0	1.977	45.86	556
3	3	1	1.814	50.24	3
4	2	2	1.614	57.00	17

3	3	3	1.522	60.81	8
5	1	1	1.522	60.81	188
4	4	0	1.398	66.86	1000
5	3	1	1.337	70.37	6
4	4	2	1.318	71.52	< 1
6	2	0	1.251	76.05	6
5	3	3	1.206	79.38	38
6	2	2	1.192	80.49	< 1
4	4	4	1.142	84.87	64
7	1	1	1.107	88.14	< 1
5	5	1	1.107	88.14	7
6	4	2	1.057	93.58	11
7	3	1	1.030	96.85	17
5	5	3	1.030	96.85	44
8	0	0	0.989	102.37	140
7	3	3	0.966	105.73	2
6	4	4	0.959	106.86	< 1
6	6	0	0.932	111.47	3
8	2	2	0.932	111.47	3
5	5	5	0.913	115.02	20
7	5	1	0.913	115.02	37
6	6	2	0.907	116.22	1
8	4	0	0.884	121.18	97
7	5	3	0.868	125.07	< 1
9	1	1	0.868	125.07	4
8	4	2	0.863	126.41	< 1
6	6	4	0.843	132.03	2
9	3	1	0.829	136.59	67

Table S4. Elemental oxides XRF assay of the Eyzies (EZ) and Standard Porcelain (SP) clays.

oxide	SiO_2	Al_2O_3	SO_3	K_2O	Rb_2O	MgO	CaO
EZ	53.6(4)	43.2(5)	0.1	-	-	1.3(4)	0.2
SP	50.4(4)	38.3(4)	0.3(1)	2.6(1)	0.1	2.3(4)	1.3(1)
oxide	SrO	BaO	TiO_2	V_2O_5	Cr_2O_3	MnO	Fe_2O_3
EZ	-	0.3	0.1	0.1	0.1	< 0.1	0.8(1)
SP	0.1	1.5(2)	0.1	-	-	0.1	2.9(1)